

Electronic Band Structure Non-linear Effects in the Stopping of Protons in Copper

Edwin E. Quashie and Bidhan C. Saha

Department of Physics, Florida A&M University, Tallahassee, FL 32307, USA

Alfredo A. Correa

Lawrence Livermore National Laboratory, 7000 East Avenue, Livermore, CA 94550, USA

We present an ab initio study of the electronic stopping power of protons in copper over a wide range of proton velocities $v = 0.01 - 10$ a.u. where we take into account non-linear effects. Time-dependent density functional theory coupled with molecular dynamics is used to study electronic excitations produced by energetic protons. A plane-wave pseudopotential scheme is employed to solve the time-dependent Kohn-Sham equations for a moving ion in a periodic crystal. These electronic excitations and the band structure determine the stopping power of the material and alter the interatomic forces for both channeling and off-channeling trajectories. Our off-channeling results are in quantitative agreement with experiments, and at low velocity they unveil a crossover region of superlinear velocity dependence (with a power of ~ 1.5) in the velocity range $v = 0.1 - 0.3$ a.u. that we associate to the copper crystalline electronic band structure. The results are rationalized by simple band models in separate regimes. We find that the limit of electronic stopping $v \rightarrow 0$ is not as simple as phenomenological models suggest and it is plagued by band-structure and non-linear effects.

The interaction of charged particles with matter has been a subject of extensive research over many decades; its results provide information for many technological applications such as nuclear safety, applied material science, medical physics and fusion and fission applications [1–4]. When a fast ion moves through a solid, it loses kinetic energy due to the excitations of the target electrons and the path of their trajectory. This energy-loss phenomenon plays an important role in many experimental studies involving radiation in solids, surfaces and nanostructures [5–11]. In particular, the condensed matter community has introduced sophisticated computer simulation techniques for this fundamentally non-adiabatic problem as spearheaded by Echenique *et al.* [12] aimed to overcome limitations of historical approaches [13–16].

In studying the role of ion-solid interactions in $H^+ + Al$, Correa *et al.* [17] have shown that the electronic excitations affects the interatomic forces relative to the adiabatic outcome. Recently Schleife *et al.* [18] have calculated the electronic stopping power (S_e) by H and He projectile including TDDFT non-adiabatic electron dynamics and found that off-channeling trajectories along with the inclusion of semicore electrons enhance S_e , resulting in better agreement with the SRIM data [19]. SRIM [19] also provides both a fitted model for electronic stopping as well as a large set of experimental points. In this case we concentrate in a metal with a richer electronic band structure around the Fermi energy, such as Cu.

The recent measurements by Cantero *et al.* [20] and by Markin *et al.* [21] of slow ($v \leq 0.6$ a.u.) H^+ in Cu give a glimpse to the extreme low velocity limit. Although disagreeing with each other in absolute scale by $\sim 40\%$ (Fig. 3), both reveal the stopping due to conduction band electronic excitations at lower velocity, evidenced as a change in slope near $v = 0.15$ or 0.10 a.u. respectively. The change of slope was deduced to be caused by the

participation of d-electrons [22].

In this Letter we will address the problem of theoretical calculation of S_e of protons in crystalline Cu in a wide range of velocities comprising the whole and beyond the range of available experimental points ($0.01 \text{ a.u.} \leq v \leq 10 \text{ a.u.}$). We perform our calculations by directly simulating the process of a proton traversing a crystal of Cu atoms, producing individual and collective electronic excitations within the TDDFT framework [17, 23, 24] including Ehrenfest molecular dynamics (EMD) [25–29]. This method is used to calculate most microscopic quantities along the process (forces, electronic density, charges, etc); in particular, we report here calculation of S_e . A quantitative explanation and interpretation of our results are furnished along with a detailed experimental comparison.

Along the simulation, we monitor the energy transferred to the electrons of the target due to a constant velocity moving proton. For simplicity, the proton is constrained to move at constant velocity, hence the total energy of the system is not conserved. The excess in total energy is instead used as a measure of the stopping power as a function of the proton velocity. As the proton moves, the time-dependent Kohn-Sham (TDKS) equation [30] describes the evolution of the electronic density and energy of the system due to the dynamics of effective single-particle states under the external potential generated by the proton and the crystal of Cu nuclei. These states are evolved in time with a self-consistent Hamiltonian that is a functional of the density:

$$i\hbar \frac{\partial}{\partial t} \psi_i(\mathbf{r}, t) = \left\{ -\frac{\hbar^2 \nabla^2}{2m} + V_{\text{KS}}[n(t), \{\mathbf{R}_J(t)\}_J](\mathbf{r}, t) \right\} \psi_i(\mathbf{r}, t) \quad (1)$$

The Kohn-Sham (KS) effective potential $V_{\text{KS}}[n(t), \{\mathbf{R}_J(t)\}_J](\mathbf{r}, t)$ is given by

$$V_{\text{KS}}[n, \{\mathbf{R}_J(t)\}_J] = V_{\text{ext}}[\mathbf{R}_J(t)\}_J] + V_{\text{H}}[n] + V_{\text{XC}}[n] \quad (2)$$

where the external potential is $V_{\text{ext}}[\{\mathbf{R}_J(t)\}_J](\mathbf{r}, t)$ due to ionic core potential (with ions at positions $\mathbf{R}_J(t)$), $V_{\text{H}}(\mathbf{r}, t)$ is the Hartree potential comprising the classical electrostatic interactions between electrons and $V_{\text{XC}}[n](\mathbf{r}, t)$ denotes the exchange-correlation (XC) potential. The spatial and time coordinates are represented by \mathbf{r} and t respectively. At time t the instantaneous density is given by $n(\mathbf{r}, t) = \sum_i |\psi_i(\mathbf{r}, t)|^2$. The XC potential used in this study is due to Perdew-Burke-Ernzerhof (PBE) [31, 32], using a norm-conserving Troullier-Martins pseudopotential, with 17 explicit electrons per Cu atom (not necessarily all 17 electrons participate in the process as we will discuss later).

Each simulation of the ion-solid collision consists of a well-defined trajectory of the projectile in the FCC metallic bulk sample with experimental density. The calculations were done using the code QBOX [33] with time-dependent modifications [23]. The Kohn-Sham (KS) orbitals are expanded in a supercell plane-wave basis. The fourth-order Runge-Kutta scheme (RK4) [23] is used to propagate these orbitals in time. The advantages of using the plane-wave approach is that it systematically deals with basis-size effects which was a drawback for earlier approaches [17, 34]. Finite-size errors in the simulations are overcome by considering large simulation cells [18].

Periodic boundary conditions are used throughout this study. The supercell size was chosen so as to reduce the specular size effects while maintaining controllable computational demands. The calculations used $(3 \times 3 \times 3)$ conventional cells containing 108 host Cu atoms and H^+ . To integrate the Brillouin zone a single k -point (Γ) was used. The basis set is sampled with a 130 Ry energy cutoff.

The projectile H^+ is initially placed in the crystal and a time-independent DFT calculation was completed to obtain the converged ground state results that are required for subsequent evolution. We then perform TDDFT calculations on the electronic system with the moving proton. Following the method introduced by Pruneda *et al.* [35] the projectile is then allowed to move with a constant velocity subjected to a straight uniform movement along a $\langle 100 \rangle$ channeling trajectory (also called hyperchanneling) which minimizes the collision of the projectile with the host atoms.

In the off-channeling case the projectile takes random trajectories through the host crystal yielding a stronger interaction between the projectile and the core of the host atom due to the larger proximity. The need to take into account off-channeling trajectories was described in Ref. [18].

Following the scheme of Ref. [23] the TDKS equation (see Eq. 1) was solved numerically with a time step of, at most, 0.121 attoseconds (which is within the numerical stability limit time-integration scheme for this basis set). High velocity points are simulated with smaller time steps. The wavefunctions were then propagated for up to tens of femtoseconds.

The total electronic energy (E) of the system changes

as a function of the projectile position (x) since the projectile (forced to maintain its velocity) deposits energy into the electronic system as it moves through the host atoms. The increase of E as a function of projectile displacement x enables us to extract the electronic stopping power as a time-averaged quantity for each velocity,

$$S_e = \overline{dE(x)/dx} \quad (3)$$

S_e has the dimension of a force (e.g. E_{h}/a_0) and it has the interpretation of a drag force acting on the projectile.

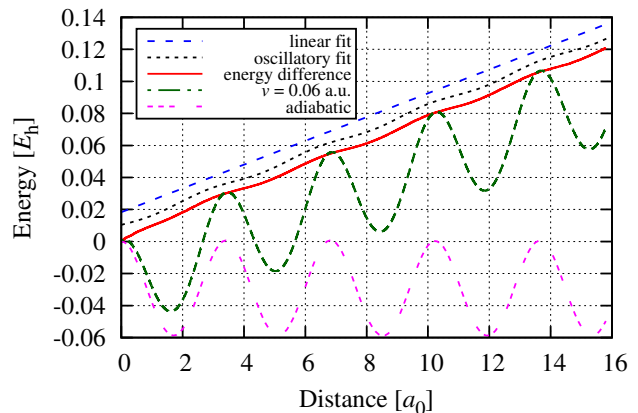


Figure 1. (color online). The increase of E as a function of proton position at velocities $v = 0.06$ a.u. (green dashed line) along $\langle 100 \rangle$ channeling trajectory and the adiabatic energy (magenta dot-dashed line). The adiabatic curve would correspond to a proton moving infinitely slowly ($v = 0$), where there is no transfer of energy, just oscillations of the total energy with a zero slope. The oscillations in the curves reflect the periodicity of the Cu lattice. The red solid line shows the energy difference (subtraction of adiabatic energy from the $v = 0.06$ a.u. curves). The blue dashed and black dotted lines shows the slope of linear and oscillatory fits of the red solid line from $x = 5.0 a_0$ (after the transient) to a given maximum position x as a function of this maximum position respectively. For visualization purposes the black line have been shifted vertically. A linear fit, $y = a + bx$ (blue line) yields a slope of $6.989 \times 10^{-3} E_{\text{h}}/a_0$ with an error of $\pm 6.936 \times 10^{-5} E_{\text{h}}/a_0$. We then proceed for a linear fit in addition to an oscillatory function $y = a + bx + A \cos(kx + \phi)$ (black dotted line) to capture any remnant oscillation. This oscillation fit generates a slope of $7.435 \times 10^{-3} E_{\text{h}}/a_0$ with an error of $\pm 8.52 \times 10^{-7} E_{\text{h}}/a_0$, that is with a very small fitting error.

In the low velocity cases extracting a slope becomes more challenging, first because a longer time simulation is required to sample the crystalline structure and second because the natural oscillations associated with the crystal periodicity becomes relatively larger. For the channeling cases, we subtract the adiabatic energy from time-dependent energy and we perform an oscillatory fit to the resulting curve. Fig. 1 explains how the slopes are evaluated in these cases. For higher velocities, a linear fit

alone is enough to obtain reasonable values with small relative errors.

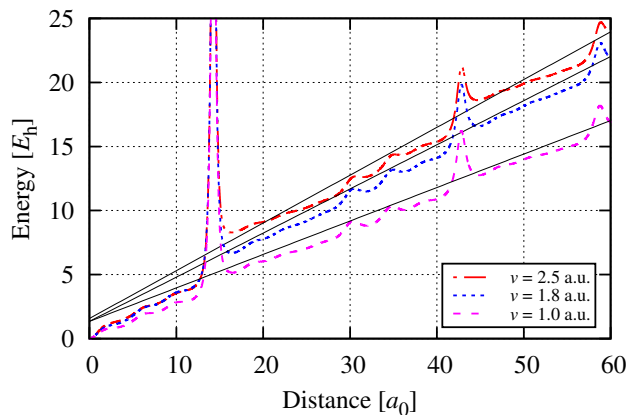


Figure 2. (color online) The total energy increase as a function of proton position at velocities $v = 1.0$ a.u. (magenta line), $v = 1.8$ a.u. (blue line) and $v = 2.5$ a.u. (red line) along the off-channeling (random direction) trajectory with corresponding linear fits (black solid lines).

For the off-channeling trajectory, the procedure for computing the S_e is depicted in Fig. 2. The sharp peaks show when the proton is in the vicinity of a host Cu atom, while the smaller peaks and flatter regions indicate that the proton is not very close to any host atom. To obtain the S_e we compute the slopes of the curves by a linear fit of the form $y = a + bx$ (black solid lines) using our data from $x > 5 a_0$ (to eliminate the transient region) to a given maximum position of x determined by minimizing reentrancy in the periodic supercell into the initial position. The slope (b) gives the electronic stopping for this off-channeling case.

Fig. 3 shows a comparison of our calculated S_e with SRIM experimental data and model. In the channeling case, when the incident velocity v increases after the maximum stopping is reached, the rate of decrease of our S_e results becomes rather faster than those obtained by either the experimental or the SRIM database.

For the off-channeling case, there is a better agreement between our S_e results with the SRIM data in most of the range. In experiments, where trajectories are not necessarily finely controlled, the projectile does indeed explore core regions of the host atoms, and that is presumably why off-channeling simulation are a better representation for the most common experiments [37]. At higher velocities ($v > 4$ a.u.) further disagreement stems from combined effect of the lack of explicit deeper core electrons in the simulation and also size effects, as excitations of long wavelength plasma oscillations are artificially constrained by the simulation supercell [18]. It is clear that a larger cell and eventually the inclusion of more core electrons would be necessary to obtain better agreement in this region.

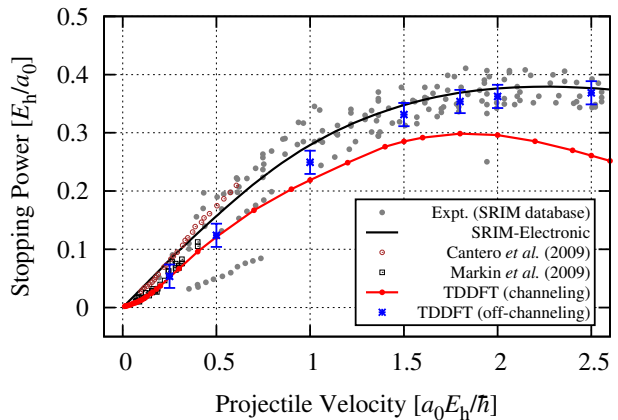


Figure 3. (color online). The S_e vs. projectile velocity v : for a channeling trajectory (red lines) and for off-channeling trajectory (blue crosses). The black continuous lines refers to the nominal tabulated results from the SRIM database for electronic stopping power [19]. The gray dots refers to the SRIM experimental database contained therein [36]. The error bars of the off-channeling trajectory are shown by the blue vertical lines, while error bars in channeling trajectories are smaller than the points. Open circles and open squares show data of Cantero *et al.* [20] and Markin *et al.* [21] respectively.

Although experimental values have considerable vertical spread, our calculated stopping power is on the low side for most of the points and also below the fitted by SRIM model [19]. While this was partially explained by taking into account off-channeling trajectories near the peak, there are possible intrinsic limitations of the approximations to the density functional theory used. Along this line we would like to note that more sophisticated approaches, based on the dielectric and current-density response but including the exact many-body and dynamic exchange-correlation treatment, are available in the literature [38]. This type of advanced approaches which are beyond the current scope of this work contain explicitly additional channels of dissipation not taken into account in our adiabatic exchange and correlation functionals, which can be relatively important. Given the aforementioned limitations of the orbital based method and the exchange and correlation used it is still reassuring to see agreement up to a few times the velocity of the maximum stopping.

We also see that at low velocity the off-channeling and channeling simulated results collapse into a common curve, this effect has been seen in the simulations before [17, 18, 39], at low velocity the effect is less sensitive to the precise geometry of the trajectory, as the geometric cross section increases.

We observe in Fig. 4 that the resulting curve is not as particularly simple. In order to interpret the results we also calculated the linear response stopping $S_L(n, v)$ [40] based on the Linhard RPA dielectric function ϵ_{RPA} for

different effective densities n of the homogeneous electron gas [41]

$$S_L(n, v) = \frac{2e^2}{\pi v^2} \int_0^\infty \frac{dk}{k} \int_0^{kv} \omega d\omega \Im \left(\frac{1}{\varepsilon_{\text{RPA}}(n, k, \omega)} \right) \quad (4)$$

(which assumes a proton effective charge of $Z_1 = 1$). As shown in Fig. 4, for $v < 0.07$ a.u. the response of the effective electron gas with one electron per Cu mimics the TDDFT results. The resulting curves in Fig. 4 shows that for $v > 0.3$ a.u. at least the 11 electrons per atom (full valence) participates in the stopping electron gas within linear response. We observe a S_e kink around $v \sim 0.07$ a.u. due to a mixture of d-band in the electronic density of states. Similarly, our new results for $v \leq 0.07$ a.u., are primarily due to s-band electrons within linear response. In the simulation we directly show a crossover region between the two linear regimes, and we find that the friction is in direct relation to the velocity with a power law with exponent 1.48 ± 0.02 .

The kink we found at $v = 0.07$ a.u. can be explained by conservation laws in the effective homogeneous electron gas and general properties of electronic density of states in crystalline Cu. The minimum energy loss with maximum momentum transfer from an electron to an ion moving with velocity v are respectively $2\hbar k_F$ and $2\hbar k_F v$ (plus corrections of order m_e/m_p). Due to Pauli exclusion, only electrons in the energy range $E_F \pm 2\hbar k_F v$ can participate in the stopping process. Taking into account that DFT band structure predicts that the d-band edge is $\Delta_{\text{DFT}} = 1.6$ eV below the Fermi energy (see for example, Fig. 3(a) in Ref. [42]), that electron (band) effective mass close to 1 and that $k_F = 0.72/a_0$ for the effective homogeneous electron gas of Cu s-electrons [43], we can derive an approximate value of v_{kink} caused by the participation of d-electrons. Based in this DFT ground state density of states plus conservation laws, we obtain an estimate of $v_{\text{kink}} = \Delta/(2\hbar k_F) = 0.41$ a.u. in qualitative agreement with the TDDFT prediction. In reality, the d-band is about $\Delta_{\text{exp}} = 2$ eV below the Fermi energy as indicated by ARPES [44], that means that both the DFT-based estimate and the TDDFT result should be giving an underestimation of 25% of the kink location. The second (negative) kink at $v = 0.3$ a.u. is more difficult to explain precisely as the qualitative description in terms of k_F (as in the homogeneous electron gas) becomes more ambiguous, but it is related to the point at which the whole conduction band (11 s + d electrons) starts participating in the process.

At low velocity, our results show good agreement with the experiments of Markin *et al.* [21] but a relative disagreement with the findings of Cantero *et al.* [20] and the SRIM model. This could be a simple experimental scaling issue related to the difference between measuring relative and absolute stopping power at low velocities [21]. We expect similar results for other transition metals, as described by Ref. [7].

Below 0.02 a.u., the lack of experimental points pre-

cludes a direct comparison, but we find a large deviation from linear behavior. One possible explanation is that bound effects break down the linear response (Lindhard) approximation that was useful to interpret the different regimes (and crossover) for velocities above 0.02 a.u.. Probing this regime experimentally would be rather difficult, especially to disentangle it from nuclear stopping effects, but if this is confirmed it would be an unexpected new regime possibly related to bound effects. In any case, the combination of experimental and theoretical results shows that the limit $v \rightarrow 0$ is intricate for metals as it is for insulators [45, 46] where analogous band and gap threshold effects have been found.

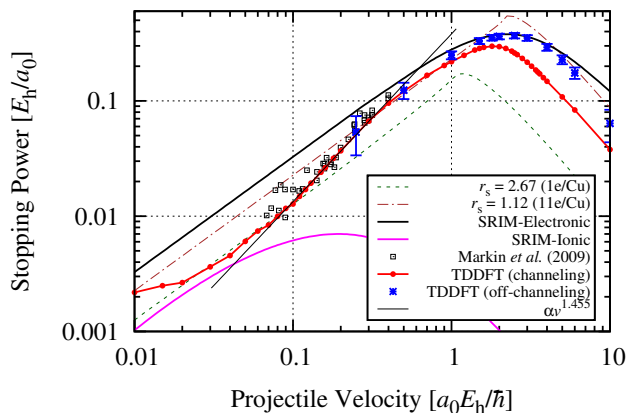


Figure 4. (color online) The average S_e vs. projectile velocity v : for a channeling trajectory (red circles) and for off-channeling trajectory (blue crosses). The solid black and solid magenta lines refer to the nominal tabulated results from the SRIM database for electronic and ionic stopping powers respectively [19]. Open squares are previous data of Markin *et al.* [21]. Dash (green) line and dash-dot (brown) line corresponds to a linear RPA calculation for a free-electron gas with $r_s = 2.67 a_0$ (1e per Cu atom) and $r_s = 1.12 a_0$ (11e per Cu atom). The thin solid black line is the polynomial curve $\propto v^q$ to fit the crossover region (with a power of $q = 1.48 \pm 0.02$).

Finally, we point out that the investigation of the low velocity limit of stopping power is important for the understanding of the non-adiabatic coupling between ions and electrons [47] and also for modeling dissipative molecular dynamics [48, 49]. In simulations of radiation events the final state is precisely controlled by dissipation in the late stages when ions move slowly but still non-adiabatically [50].

In summary, in this Letter we have reported the S_e of protons in copper in a very wide range of velocities. TDDFT-based electron dynamics is capable of capturing most of the physics in the different ranges, starting from non-linear screening effects, electron-hole excitations and production of plasmons. We disentangled channeling and off-channeling effects and observe a collapse of the two curves at low velocities; and identified five regimes i) the linear s-only (0.02–0.07 a.u.), ii) linear s+d (0.3–1 a.u.),

iii) crossover with ~ 1.5 -power law (0.07 – 0.3 a.u.), iv) plasmon-like ($v > 1$ a.u.) and v) what is possibly a non-linear screening regime at $v < 0.02$ a.u.. This is a further illustration that the electronic stopping in general does not possess a simple behavior in the limit $v \rightarrow 0$, and that band and bound effects dominate this behavior.

We would like to thank Professor C. A. Weatherford, Dr. E. R. Schwegler and Dr. K. J. Reed for their keen interests, constant encouragements and useful suggestions throughout the progress of this work. This work was

performed under the auspices of the U.S. Department of Energy by Lawrence Livermore National Laboratory under Contract DE-AC52-07NA27344. Computing support for this work came from the Lawrence Livermore National Laboratory Institutional Computing Grand Challenge program. This is a collaborative project between the Department of Physics, Florida A&M University and Lawrence Livermore National Laboratory. E. E. Quashie and B. C. Saha thankfully acknowledge the support by National Nuclear Security Administration (NNSA) grant.

-
- [1] F. F. Komarov, A. F. Komarov, V. V. Pil'ko, and V. V. Pil'ko, *J Eng Phys Thermophy* **86**, 1481 (2013).
- [2] P. Patel, A. Mackinnon, M. Key, T. Cowan, M. Ford, M. Allen, D. Price, H. Ruhl, P. Springer, and R. Stephens, *Phys. Rev. Lett.* **91** (2003), 10.1103/physrevlett.91.125004.
- [3] G. J. Caporaso, Y.-J. Chen, and S. E. Sampayan, *Reviews of Accelerator Science and Technology* **02**, 253 (2009).
- [4] G. R. Odette and B. D. Wirth, in *Handbook of Materials Modeling* (Springer Netherlands, 2005) pp. 999–1037.
- [5] S. Chenakin, S. Markin, E. Steinbauer, M. Draxler, and P. Bauer, *Nuclear Instruments and Methods in Physics Research Section B: Beam Interactions with Materials and Atoms* **249**, 58 (2006).
- [6] E. A. Figueroa, E. D. Cantero, J. C. Eckardt, G. H. Lantschner, J. E. Valdés, and N. R. Arista, *Phys. Rev. A* **75** (2007), 10.1103/physreva.75.019905.
- [7] S. N. Markin, D. Primetzhofer, S. Prusa, M. Brunmayr, G. Kowarik, F. Aumayr, and P. Bauer, *Phys. Rev. B* **78** (2008), 10.1103/physrevb.78.195122.
- [8] M. Kaminsky, in *Atomic and Ionic Impact Phenomena on Metal Surfaces* (Springer Science + Business Media, 1965) pp. 142–237.
- [9] C. Lehmann and D. G. Doran, *Phys. Today* **31**, 70 (1978).
- [10] P. Sigmund, *Particle Penetration and Radiation Effects Volume 2* (Springer International Publishing, 2014).
- [11] M. Nastasi, J. Mayer, and J. K. Hirvonen, in *Ion-solid Interactions* (Cambridge University Press (CUP), 1996) pp. 88–114.
- [12] P. M. Echenique, I. Nagy, and A. Arnau, *Int. J. Quantum Chem.* **36**, 521 (1989).
- [13] H. Bethe, *Ann. Phys.* **397**, 325 (1930).
- [14] F. Bloch, *Ann. Phys.* **408**, 285 (1933).
- [15] E. Fermi and E. Teller, *Phys. Rev.* **72**, 399 (1947).
- [16] J. Lindhard and A. Winther, *Kgl. Danske Videnskab. Selskab. Mat. Fys. Medd.* **34** (1964).
- [17] A. A. Correa, J. Kohanoff, E. Artacho, D. Sanchez-Portal, and A. Caro, *Phys. Rev. Lett.* **109** (2012), 10.1103/physrevlett.109.069901.
- [18] A. Schleife, Y. Kanai, and A. A. Correa, *Phys. Rev. B* **91** (2015), 10.1103/physrevb.91.014306.
- [19] J. F. Ziegler, M. Ziegler, and J. Biersack, *Nuclear Instruments and Methods in Physics Research Section B: Beam Interactions with Materials and Atoms* **268**, 1818 (2010).
- [20] E. D. Cantero, G. H. Lantschner, J. C. Eckardt, and N. R. Arista, *Phys. Rev. A* **80** (2009), 10.1103/physreva.80.032904.
- [21] S. N. Markin, D. Primetzhofer, M. Spitz, and P. Bauer, *Phys. Rev. B* **80** (2009), 10.1103/physrevb.80.205105.
- [22] D. Goebel, D. Roth, and P. Bauer, *Phys. Rev. A* **87** (2013), 10.1103/physreva.87.062903.
- [23] A. Schleife, E. W. Draeger, Y. Kanai, and A. A. Correa, *The Journal of Chemical Physics* **137**, 22A546 (2012).
- [24] A. Schleife, E. W. Draeger, V. M. Anisimov, A. A. Correa, and Y. Kanai, *Comput. Sci. Eng.* **16**, 54 (2014).
- [25] E. K. U. Gross, J. F. Dobson, and M. Petersilka, in *Density Functional Theory II* (Springer Science + Business Media, 1996) pp. 81–172.
- [26] F. Calvayrac, P.-G. Reinhard, E. Suraud, and C. Ullrich, *Physics Reports* **337**, 493 (2000).
- [27] D. R. Mason, J. le Page, C. P. Race, W. M. C. Foulkes, M. W. Finnis, and A. P. Sutton, *Journal of Physics: Condensed Matter* **19**, 436209 (2007).
- [28] J. L. Alonso, X. Andrade, P. Echenique, F. Falceto, D. Prada-Gracia, and A. Rubio, *Phys. Rev. Lett.* **101** (2008), 10.1103/physrevlett.101.096403.
- [29] X. Andrade, A. Castro, D. Zueco, J. L. Alonso, P. Echenique, F. Falceto, and A. Rubio, *J. Chem. Theory Comput.* **5**, 728 (2009).
- [30] E. Runge and E. K. U. Gross, *Phys. Rev. Lett.* **52**, 997 (1984).
- [31] J. P. Perdew and Y. Wang, *Physical Review B* **45**, 13244 (1992).
- [32] J. P. Perdew, K. Burke, and M. Ernzerhof, *Phys. Rev. Lett.* **77**, 3865 (1996).
- [33] F. Gygi, *IBM Journal of Research and Development* **52**, 137 (2008).
- [34] J. M. Pruneda, D. Sánchez-Portal, A. Arnau, J. I. Juaristi, and E. Artacho, *Phys. Rev. Lett.* **99** (2007), 10.1103/physrevlett.99.235501.
- [35] J. M. Pruneda and E. Artacho, *Phys. Rev. B* **71** (2005), 10.1103/physrevb.71.094113.
- [36] <http://www.srim.org/SRIM/SRIMPICS/STOP01/STOP0129.gif>.
- [37] J. J. Dorado and F. Flores, *Phys. Rev. A* **47**, 3062 (1993).
- [38] V. U. Nazarov, J. M. Pitarke, Y. Takada, G. Vignale, and Y.-C. Chang, *Phys. Rev. B* **76** (2007), 10.1103/physrevb.76.205103.
- [39] R. Ullah, F. Corsetti, D. Sánchez-Portal, and E. Artacho, *Phys. Rev. B* **91** (2015), 10.1103/physrevb.91.125203.
- [40] J. Lindhard, A. Winther, and K. D. videnskabernes selskab, *Stopping Power of Electron Gas and Equipartition Rule*, *Mathematisk-fysiske meddelelser* (Munksgaard, 1964).
- [41] G. Giuliani and G. Vignale, in *Quantum Theory of the*

- Electron Liquid* (Cambridge University Press (CUP), 2005) pp. 188–274.
- [42] Z. Lin, L. V. Zhigilei, and V. Celli, *Phys. Rev. B* **77** (2008), 10.1103/physrevb.77.075133.
- [43] N. W. Ashcroft and N. D. Mermin, *Solid State Physics* (Thomson Press (India) Ltd, 2003).
- [44] J. A. Knapp, F. J. Himpsel, and D. E. Eastman, *Phys. Rev. B* **19**, 4952 (1979).
- [45] E. Artacho, *Journal of Physics: Condensed Matter* **19**, 275211 (2007).
- [46] A. Lim, W. M. C. Foulkes, A. P. Horsfield, D. R. Mason, A. Schleife, E. W. Draeger, and A. A. Correa, *Phys. Rev. Lett.* (in press) (2015).
- [47] A. Caro, A. A. Correa, A. Tamm, G. D. Samolyuk, and G. M. Stocks, *Phys. Rev. B* **92** (2015), 10.1103/physrevb.92.144309.
- [48] A. Caro and M. Victoria, *Phys. Rev. A* **40**, 2287 (1989).
- [49] D. M. Duffy and A. M. Rutherford, *Journal of Physics: Condensed Matter* **19**, 016207 (2006).
- [50] E. Zarkadoula, S. L. Daraszewicz, D. M. Duffy, M. A. Seaton, I. T. Todorov, K. Nordlund, M. T. Dove, and K. Trachenko, *Journal of Physics: Condensed Matter* **26**, 085401 (2014).